Tris(pyrazolyl)methanesulfonates: More Than Just Analogues of Tris(pyrazolyl)borate Ligands; N,N,N-, N,N,O-, and Other Coordination Modes

Wolfgang Kläui,*[a] Michael Berghahn,[a] Walter Frank,[a] Guido J. Reiß,[a] Thomas Schönherr,[b] Gerd Rheinwald,[c] and Heinrich Lang[c]

Dedicated to Professor Rüdiger Mews on the occasion of his 60th birthday

Keywords: Enzyme models / N,O ligands / Transition metals / Tripodal ligands

The thallium(I) salts of tris(pyrazolyl)methanesulfonate (Tpms) and tris(3-*tert*-butylpyrazolyl)methanesulfonate (Tpms^{tBu}) have been used to prepare the following complexes: [(Tpms^{tBu})ZnX] [X = Cl (**1a**), Br (**1b**), I (**1c**), Et (**3**), OAc (**5a**)], [(Tpms^{tBu})NiX] [X = Cl (**2a**), Br (**2b**)], [(Tpms^{tBu})-CoCl(Hpz^{tBu})] (**3**), [(Tpms^{tBu})Zn(μ-OAc)(μ-OH)Zn(Tpms^{tBu})] (**5b**), [(Tpms^{tBu})Cu(CO)] (**6a**), and [(Tpms)Cu(CO)] (**6b**). The solid-state structures of **1b**, **2a**, **3**, and **5b** have been determined by X-ray analysis. The optical spectra of **2a** and **3** were investigated by means of the angular overlap model to elucidate their electronic structures in view of the underlying molecular geometries. Variable-temperature NMR and IR spectroscopic studies show that Tpms and Tpms^{tBu} can act as N,N,N and N,N,O ligands. Both coordination modes are present in solution for the zinc complexes **1a**,**b** and the copper carbonyl complexes **6a**,**b**. The N,N,O bonding mode is entropically favoured in solution. For the nickel complexes **2a**,**b**, the Tpms^{tBu} ligand acts as a tripodal nitrogen ligand in the solid state and in solution. For the dinuclear zinc complex **5b**, one of the Tpms^{tBu} ligands acts as an N,N,O ligand and one as an N,O ligand. Complex **5b** is one of the very few structural models of the dinuclear zinc enzymes phospholipase C and phosphotriesterase.

Introduction

Recently we reported the synthesis of the tris(pyrazolyl)-methanesulfonates (Tpms), a novel class of ligands.[1] These ligands were designed by analogy to the well-known tris-(pyrazolyl)borate (Tp) ligands.[2] They have the same nitrogen-donor set as the Tp ligands, but in addition they bear a sulfonate group to make the ligands more hydrophilic.

Herein we describe the coordination behaviour of the sterically demanding ligand tris(3-*tert*-butylpyrazolyl)methanesulfonate (Tpms^{tBu}) (Figure 1) towards zinc(II), nickel(II), cobalt(II), and copper(I) ions, as well as the structural flexibility and the dynamic stereochemistry of this ligand.

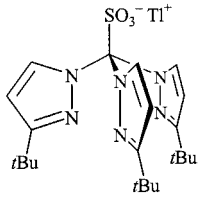

Figure 1. Schematic structure of the thallium salt of the Tpms^{tBu} ligand

Results and Discussion

1. The Complexes [(Tpms^{tBu})ZnX] (1) and [(Tpms^{tBu})NiX] (2) (X = Halide)

The complexes [(Tpms^{tBu})MX] were synthesised by reaction of TlTpms^{tBu} with the appropriate metal halide at room temperature [Equation (1)]. In contrast to the analogous Tp^{tBu} complexes,[3] these Tpms^{tBu} complexes have good solubility in polar solvents like wet methanol.

$$TlTpms^{tBu} + MX_2 \longrightarrow [Tpms^{tBu}MX] + TlX \quad (1)$$

[a] Institut für Anorganische Chemie und Strukturchemie der Universität Düsseldorf,
Universitätsstraße 1, 40225 Düsseldorf, Germany
E-mail: klaeui@uni-duesseldorf.de
[b] Institut für Theoretische Chemie der Universität Düsseldorf,
Universitätsstraße 1, 40225 Düsseldorf, Germany
[c] Lehrstuhl für Anorganische Chemie, Technische Universität Chemnitz,
Straße der Nationen 62, 09107 Chemnitz, Germany

The Solid-State and Solution Structures of [(Tpms^{tBu})ZnX] [X = Cl (1a), Br (1b), I (1c)]

The sterically demanding ligand Tp^{tBu} stabilises almost exclusively ions with coordination number four ("tetrahedral enforcer"[4]) and forms complexes with the composition [Tp^{tBu}MX]. In the case of **1a**−**c**, the analogous composition [(Tpms^{tBu})ZnX] is found, but the ^{1}H NMR spectra in $CDCl_3$ do not show the expected pattern of signals. Three different sets of pyrazolyl signals are found for **1a** and **1b**.

Variable-temperature NMR studies of **1a** and **1b** show that two of the three sets of signals occur in an intensity ratio of 1:2 at all temperatures (Figure 2). This ratio indicates that an equilibrium between two different species exists in solution: the expected C_{3v}-symmetrical complex and a C_s-symmetrical complex (Scheme 1). In the C_s-symmetrical species, Tpms^{tBu} coordinates with two nitrogen atoms and one oxygen atom of the sulfonate group, i.e. the ligand acts as an N,N,O ligand.

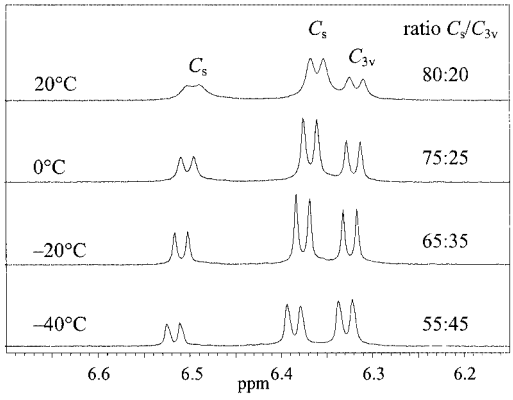

Figure 2. ^{1}H NMR spectra (200 MHz) of **1a** (pyrazolyl 4-*H* region) in $CDCl_3$ in the temperature range −40 to +20 °C

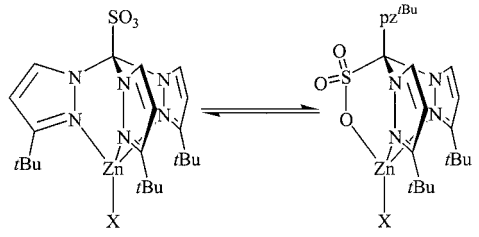

Scheme 1. Equilibrium between a C_{3v}- and a C_s-symmetrical zinc halide complex in solution (X = Cl, Br)

The ^{1}H NMR spectrum of **1c** shows only the signals for the C_s-symmetrical complex. Even at low temperatures the C_{3v}-symmetrical complex cannot be detected.

Obviously the sulfonate group, which was introduced to increase the solubility in polar solvents, is a competing donor centre. This result was surprising since the sulfonate unit is regarded as a weakly coordinating group, especially in comparison with nitrogen atom donors.[5]

Having the results of the variable-temperature studies at hand, we calculated the equilibrium constant $K = c[C_s]/c[C_{3v}]$ for **1a**. The enthalpy and entropy of the transformation of the C_{3v}-symmetrical into the C_s-symmetrical species were determined from a van't Hoff plot. In chloroform, the C_{3v}-symmetrical species is favoured enthalpically ($\Delta H = +8.0$ kJ·mol^{-1}), but the entropy of the transformation is positive: $\Delta S = +40$ J·K^{-1}·mol^{-1}. As a result, the C_s-symmetrical complex is the dominant isomer in the studied temperature range. The C_s isomer is favoured entropically per se because of its lower symmetry. We assume, however, that the rather large positive entropy is a result of the smaller dipole moment of the C_s-symmetrical complex, which allows the solvent to be more disordered.

Compound **1b** crystallises from THF/pentane in the monoclinic space group $P2_1/c$. The asymmetric unit of the crystal structure contains two complexes with very similar structures and one molecule of THF. The ZORTEP plot given in Figure 3 shows one of the symmetry-independent complexes. Selected bond lengths and angles are summarised in Table 1.

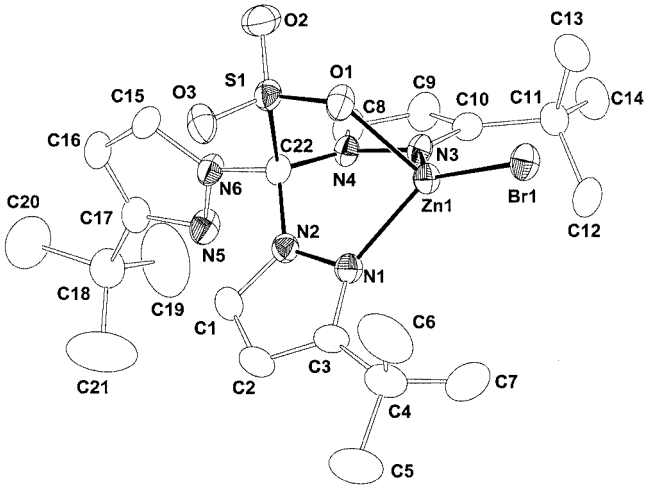

Figure 3. ZORTEP plot of [(Tpms^{tBu})ZnBr] (**1b**)

The zinc atom is coordinated in a distorted tetrahedral geometry. In the solid state, the Tpms^{tBu} ligand coordinates as an N,N,O ligand.

Recently, Burzlaff published the structure of a zinc complex containing a similar monoanionic N,N,O ligand derived from bis(pyrazolyl)acetic acid. It is a model compound for zinc enzymes with the facially coordinating 2-His-1-carboxylate triad, such as thermolysin and carboxypeptidase.[6] The Zn−O bond lengths show that the sulfonate group is a weaker donor than the carboxylate group. Burzlaff observed a Zn−O bond length of 1.990(2) Å, which is significantly shorter than in **1b** [2.017(2) Å]. The Zn−O distances in thermolysin (2.08 Å) and carboxypeptidase (2.2 Å) are very similar to the Zn−O distance of compound **1b**.[6]

Table 1. Selected bond lengths [Å] and angles [°] in [(Tpms^{tBu})ZnBr] (**1b**)

Zn1−N3	2.014(2)	Zn2−N9	2.025(2)
Zn1−O1	2.017(2)	Zn2−O4	2.032(2)
Zn1−N1	2.048(2)	Zn2−N7	2.054(2)
Zn1−Br1	2.2905(4)	Zn2−Br2	2.2778(5)
S1−O2	1.426(2)	S2−O5	1.431(2)
S1−O3	1.435(2)	S2−O6	1.437(2)
S1−O1	1.463(2)	S2−O4	1.470(2)
S1−C22	1.885(3)	S2−C44	1.880(3)
N3−Zn1−O1	91.73(9)	N9−Zn2−O4	92.89(9)
N3−Zn1−N1	90.42(9)	N9−Zn2−N7	89.39(10)
O1−Zn1−N1	91.13(9)	O4−Zn2−N7	91.25(9)
N3−Zn1−Br1	131.13(7)	N9−Zn2−Br2	134.66(7)
O1−Zn1−Br1	108.04(6)	O4−Zn2−Br2	108.55(6)
N1−Zn1−Br1	131.74(7)	N7−Zn2−Br2	128.08(7)
O2−S1−O3	117.88(14)	O5−S2−O6	117.37(14)
O2−S1−O1	112.35(13)	O5−S2−O4	113.41(13)
O3−S1−O1	112.81(14)	O6−S2−O4	112.25(14)
O2−S1−C22	105.27(14)	O5−S2−C44	104.76(13)
O3−S1−C22	103.17(13)	O6−S2−C44	104.63(13)
O1−S1−C22	103.48(12)	O4−S2−C44	102.50(12)

Structural Studies on [(Tpms^{tBu})NiX], X = Cl (2a), Br (2b)

To see the influence of the nature of the metal ion on the coordination behaviour of the Tpms^{tBu} ligand, we prepared the nickel complexes [(Tpms^{tBu})NiX] (**2a**: X = Cl; **2b**: X = Br) by analogy to the zinc complexes **1a**−**c**. The crystal structure of **2a** was determined. The complex crystallises from THF/pentane in the monoclinic space group $P2_1/n$. Figure 4 shows an ORTEP plot of **2a**. Selected bond lengths and angles are summarised in Table 2.

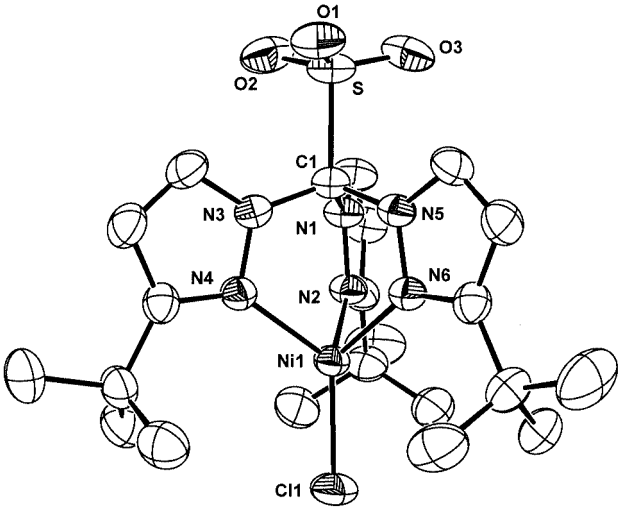

Figure 4. ORTEP plot of [(Tpms^{tBu})NiCl] (**2a**)

In contrast to the above-mentioned zinc complexes, Tpms^{tBu} coordinates to the nickel ion through the three pyrazolyl nitrogen atoms and forms a complex with C_{3v}-symmetry. This coordination is the same N,N,N mode as observed in the C_s-symmetrical trigonal-bipyramidal rhodium complex [(Tpms)Rh(nbd)], the structure of which we have recently determined.[7]

Table 2. Selected bond lengths [Å] and angles [°] in [(Tpms^{tBu})NiCl] (**2a**)

Ni1−N2	2.0088(13)	N2−Ni1−N6	90.06(5)
Ni1−N6	2.0105(14)	N2−Ni1−N4	90.12(5)
Ni1−N4	2.0105(13)	N6−Ni1−N4	89.66(5)
Ni1−Cl1	2.1746(6)	N2−Ni1−Cl1	124.24(4)
S1−O1	1.4380(15)	N6−Ni1−Cl1	125.30(4)
S1−O2	1.4433(16)	N4−Ni1−Cl1	126.35(4)
S1−O3	1.4452(15)	O1−S1−O2	115.04(10)
S1−C1	1.9283(15)	O1−S1−O3	115.98(9)
		O2−S1−O3	115.92(9)
		O1−S1−C1	102.44(8)
		O2−S1−C1	102.26(8)
		O3−S1−C1	101.96(8)

The nickel centre is coordinated in a trigonally distorted tetrahedral geometry. This arrangement is apparent from the N−Ni−Cl angles [124.24(4)−126.35(4)°] and in the smaller N−Ni−N angles [89.66(5)−90.12(5)°]. The distortion is similar to that observed for the [Tp^{tBu}MX] complexes.[8] The UV/Vis spectra of **2a** in dichloromethane and tetrahydrofuran solution, and in the solid state, are identical, and therefore we propose the same coordination mode of the Tpms^{tBu} ligand in solution as is observed in the solid state. The spectrum of **2b** in solution is slightly shifted bathochromically, but shows the same pattern as the spectrum of **2a**; therefore, an analogous structure can be assumed for **2b**. Both compounds are intensively red, an unusual colour for tetrahedral nickel(II) complexes. To obtain a better understanding of their colour, we have analysed the UV/Vis spectra in terms of the Angular Overlap Model (AOM) (see below).

2. Structural Studies on [(Tpms^{tBu})CoCl(Hpz^{tBu})] (3), a Five-Coordinate Cobalt(II) Complex

In bioinorganic chemistry it is often possible to probe the metal environment in zinc-containing enzymes with a cobalt ion as a substitute for the native zinc ion. This substitution can be misleading, however, because of the slightly different tendencies of cobalt(II) and zinc(II) ions to prefer tetrahedral vs. trigonal-bipyramidal coordination.[9] We wanted, therefore, to compare the coordination behaviour of Tpms^{tBu} towards zinc and cobalt chloride.

The reaction of TlTpms^{tBu} with cobalt chloride leads to a blue complex with the composition [(Tpms^{tBu})CoCl(Hpz^{tBu})] (**3**). The UV/Vis spectrum of this compound in dichloromethane exhibits its major band in the range 520−603 nm with an absorption coefficient ε_{max} = 402 $M^{-1}\cdot cm^{-1}$. This band shows the same pattern as the major band of the five-coordinate complex [Tp^{tBu}Co(η^2-NO_3)] (517−600 nm, ε_{max} = 212 $M^{-1}\cdot cm^{-1}$ in THF) published by Parkin.[8] Obviously a five-coordinate complex has formed rather than the expected four-coordinate halide complex.

Complex **3** crystallises from THF/pentane in the monoclinic space group $P2_1/n$ and the asymmetric unit of the crystal structure contains one molecule of THF. The ORTEP plot is given in Figure 5. Selected bond lengths and angles are summarised in Table 3.

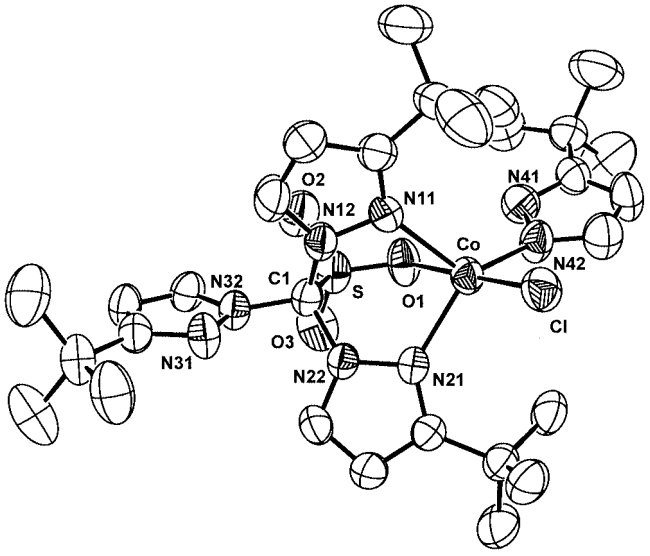

Figure 5. ORTEP plot of [(Tpms^{tBu})CoCl(Hpz^{tBu})] (**3**)

Table 3. Selected bond lengths [Å] and angles [°] in [(Tpms^{tBu})-CoCl(Hpz^{tBu})] (**3**)

Co−N42	2.035(3)	N42−Co−C1	97.49(10)
Co−N21	2.051(3)	N21−Co−C1	103.89(8)
Co−N11	2.094(3)	N11−Co−C1	103.88(8)
Co−C1	2.2738(12)	N42−Co−O1	78.51(11)
Co−O1	2.355(2)	N21−Co−O1	77.94(10)
S−O3	1.421(3)	N11−Co−O1	79.52(10)
S−O2	1.430(3)	Cl−Co−O1	175.81(7)
S−O1	1.453(2)	O3−S−O2	116.62(19)
S−C1	1.879(3)	O3−S−O1	113.99(18)
		O2−S−O1	113.61(18)
N42−Co−N21	28.33(12)	O3−S−C1	103.67(16)
N42−Co−N11	123.07(11)	O2−S−C1	104.43(16)
N21−Co−N11	96.63(10)	O1−S−C1	102.28(14)

The Tpms^{tBu} ligand coordinates in the N,N,O mode. The coordination sphere is completed by a chloro ligand and a pyrazole ligand, which derives from partial hydrolysis of the Tpms^{tBu} ligand. This hydrolysis cannot be avoided, even by using thoroughly dried anhydrous cobalt(II) chloride. This observation is noteworthy because the hygroscopic $ZnCl_2$ used for the synthesis of **1a** contained significant amounts of water, but in this case no hydrolysis occurred. The formation of **3** shows the different reactivity of cobalt and zinc ions. We have observed a similar difference in the coordination behaviour of cobalt and zinc ions towards the Tp^{Ph} ligand.[9]

The crystal structure analysis shows that the cobalt(II) ion in **3** has a distorted trigonal-bipyramidal coordination geometry. The coordinated oxygen atom of the tripodal ligand and the chloro ligand occupy the axial positions. Two pyrazolyl rings of the Tpms^{tBu} ligand and the free pyrazole are in the equatorial positions. The Co−O bond [2.355(2) Å] is significantly longer than those of Co^{II}−sulfonate complexes cited in the Cambridge Crystallographic Database [coordination number (CN) 5: 2.06 Å; CN 6: 1.94−2.22 Å].[10]

As the sulfonate group is less bulky than a *tert*-butylpyrazolyl group, Tpms^{tBu} does not prevent coordination numbers higher than four from forming when it acts as an N,N,O ligand. This effect allows the additional coordination of a ligand such as the *tert*-butylpyrazol unit.

The five-coordinate cobalt(II) complex **3** has the intensive blue colour that we had expected for a four-coordinate cobalt(II) complex. Since no ligand-field analysis of the novel ligand Tpms^{tBu} has been carried out until now, we analysed the UV/Vis spectrum of the cobalt complex **3** together with the spectrum of the tetrahedral nickel complex **2a** (see above) in terms of the Angular Overlap Model, hoping for a consistent picture of the ligand-field properties of this ligand.

3. AOM Analysis of the UV/Vis Spectra of the (Tpms^{tBu})Ni^{II} and -Co^{II} Complexes 2a and 3

The Angular Overlap Model (AOM) has been shown to be a powerful tool for rationalising d^n-level splittings in low-symmetry transition metal complexes.[11] Its advantage over the conventional ligand-field theory emerges from explicitly accounting the specific angular geometry of the chromophore, as well as involving peculiarities of the metal−ligand bonding. The latter is achieved by introducing *local* metal−ligand interaction parameters of σ and π type, which are often transferable between similar transition metal complexes. In this section we investigate the optical spectra of [(Tpms^{tBu})NiCl] (**2a**) and [(Tpms^{tBu})-CoCl(Hpz^{tBu})] (**3**) by means of the AOM to elucidate their electronic structures in view of the underlying molecular geometries.

[(Tpms^{tBu})NiCl] (2a)

In a tetrahedral ligand field, the d^8 system of Ni^{II} gives rise to a $^3T_1$ (^3F) ground state and $^3T_2$ (^3F), $^3A_2$ (^3F), and $^3T_1$ (^3P) excited states. The optical spectrum is dominated by the spin-allowed transition $^3T_1$ (^3F) → $^3T_1$ (^3P), typically located in the region 14000−17000 cm^{-1}, whereas the other triplets are expected in the near-infrared (4000−11000 cm^{-1}).[12] As so far, the present complex **2a** shows the typical absorption pattern, which is depicted in Figure 6, though the band maxima are significantly shifted to lower wavelengths. This observation is particularly true when compared with the closely related complex [Tp^{tBu}NiCl]:[8] The main absorption, which reflects the respective colour of a complex, is shifted from 505 nm (purple) to 475 nm (red), the latter being a rather uncommon colour for tetrahedrally coordinated nickel(II) complexes. The reason for the hypsochromic shift is not clear at first glance.

To elucidate this situation, we have measured spectra of microcrystalline powders, where a better resolved band structure was obtained on cooling down to liquid helium temperatures. Band maxima, on the other hand, are only slightly shifted, which excludes a solvent effect being responsible for the red colour of [(Tpms^{tBu})NiCl]. A deeper

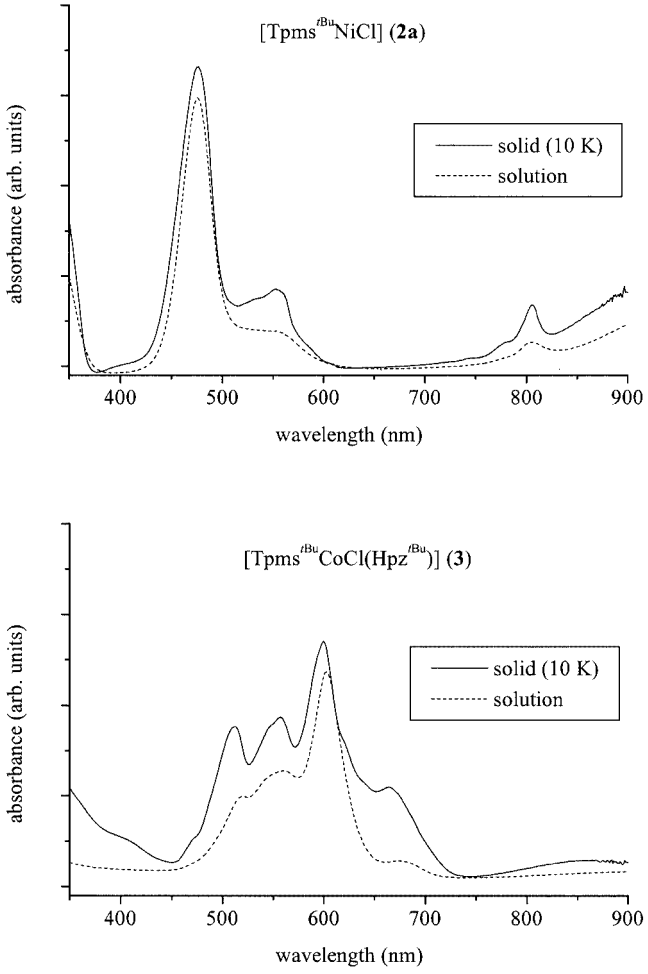

Figure 6. UV/Vis spectra of [(Tpms^{tBu})NiCl] (**2a**) and [(Tpms^{tBu})-CoCl(Hpz^{tBu})] (**3**) in solution (dichloromethane) and in the solid state

look into the electronic structure reveals that the underlying trigonal symmetry is the reason for the higher transition energies according to $^3T_1$ (^3F) → $^3T_1$ (^3P) and $^3T_1$ (^3F) → $^3A_2$ (^3F). We note that further band splittings are expected by the effect of spin-orbit coupling present in Ni^{II} complexes. Such information, however, is not available, even from the better resolved low-temperature spectrum. Moreover, from our AOM calculations, we have found such splittings and band shifts to be significantly smaller than those resulting from the geometrical effect. Therefore we restrict the following discussion to the analysis of the LS states.

The orbitally triply degenerate states split under the influence of the local trigonal symmetry, which is reflected, for example, in the large splitting of about 3000 cm^{-1} for the intense $^3T_1$ (^3P) band. A deconvolution of the band shape yields maxima at 474 nm and 556 nm, which are due to the transitions $^3A_2$ (^3F) → $^3A_2$ (^3P) and $^3A_2$ (^3F) → ^3E (^3P), respectively (in the notation of the C_{3v} group). The transition into $^3A_2$ (^3F) is located at 805 nm (12400 cm^{-1}), again somewhat higher in energy than observed for other pseudo-tetrahedrally coordinated nickel compounds. Besides these absorptions, the low-temperature spectrum exhibits several spin-forbidden transitions into singlet states that result from ^1D (^1E, $^1T_2$) and the higher ^1G ($^1T_2$, $^1A_1$, $^1T_1$, ^1E) multiplets. This manifold of experimentally available data provides a sound base for a reliable AOM analysis of the d-states involved. It turns out that the hypsochromic band shift has a simple geometrical background: When comparing the angular structure of the chromophore of [(Tpms^{tBu})NiCl] determined here with those of the related complexes [Tp^{tBu}MCl] (M = Zn, Cu, Ni, Fe, Co),[8,13] we recognize larger angles Cl−M−N for the complex under investigation (close to 125°) than for any of the Tp^{tBu} compounds (mean values around 121°). The trigonal elongation causes the considerable splitting of the orbitally degenerate triplet states together with a lowering of the ground-state energy that is responsible for the higher transition energies in [(Tpms^{tBu})NiCl]. To prove this result, we performed a complete analysis for all the d-states, which are accessible from the low-temperature absorption spectrum. In the optimization procedure, all underlying AOM parameters, i.e. e_σ^{Cl}, e_σ^{pz}, e_π^{Cl}, $e_{\pi\perp}^{pz}$, were freely optimized as were also the Racah parameters *B* and *C* that describe the electron−electron interaction.[14] While anisotropic π interaction requires, in general, two independent AOM parameters ($e_{\pi\|}$ and $e_{\pi\perp}$) for considering contributions parallel and perpendicular to the chelate plane, the in-plane π interaction with the pyrazole group is small and can be reasonably neglected here as for ammine and sp^2-hybridized amine complexes ($e_{\pi\|}^{pz} = 0$). All calculations were performed with the AOMX programme,[14] which is available in the internet (www.aomx.de). The result of our optimization procedure is presented in Table 4. Herein we used different weighting factors to distinguish spin-allowed from spin-forbidden transitions, since the band maxima of the latter have been located by a deconvolution procedure. The underlying electronic parameters are collected in Table 5. For identifying the eigenstates, the geometry was kept trigonal by taking a value of 125° for all three Cl−Ni−N angles. This restriction does not weaken the analysis, because further splittings of degenerate E states are not observed in the low-temperature absorption spectrum [the small absorption at 13500 cm^{-1} may be due to spin-orbit effects and/or the low-symmetry splitting of ^1E (^1D)].

In summary, the AOM analysis clearly demonstrates that all details obtained from the optical spectrum can be rationalized. The derived parameter values are reasonable and their positive values prove the expected antibonding behaviour. Because of an unfavorable relationship between experimental data (eight) and fitted parameters (six), clear-cut decisions about the presented parameter values should not be made on this stage. They may, nevertheless, serve as a useful estimation for future investigations of similar compounds.

[(Tpms^{tBu})CoCl(Hpz^{tBu})] (3)

The situation with the cobalt compound is rather different. The structural investigation exhibits coordination number five and a strongly distorted geometry with absence of

Table 4. Experimental and calculated d−d transition energies for [(Tpms^{tBu})NiCl] (**2a**) (in cm^{-1})

Excited state (C_{3v})	Parent state (T_d)	Energy (exp.)	Energy (calcd.)	Difference	Weight
$^3A_2$ [a]	$^3T_1$ (^3F)	0[a]	0[a]		
^3E	$^3T_1$ (^3F)		5240		
$^3A_1$	$^3T_2$ (^3F)		7690		
^3E	$^3T_2$ (^3F)		10100		
^3A	**$^3A_2$ (^3F)**	**12420**	**12350**	**70**	**1.0**
^1E	^1E (^1D)	12830[b]	12390	440	0.2
^1E	$^1T_2$ (^1D)	17250	17130	120	0.2
^3E	**$^3T_1$ (^3P)**	**18050**	**18060**	**10**	**1.0**
$^1A_1$	$^1T_2$ (^1D)	18500	18360	140	0.2
$^1A_1$	$^1T_2$ (^1G)	19300	19790	49	0.2
^3A	**$^3T_1$ (^3P)**	**21100**	**21090**	**10**	**1.0**
^1E	$^1T_2$ (^1G)	sh [c]	22070		
$^1A_1$	$^1A_1$ (^1G)	sh [c]	23260		
$^1A_1$	$^1T_1$ (^1G)	25200	25010	190	0.2
^1E	$^1T_1$ (^1G)	25200	25580	380	0.2
^1E	^1E (^1G)		29430		

[a] Ground state. [b] The small absorption at 13500 cm^{-1} may be due to spin-orbit effects and/or the low-symmetry splitting of ^1E (^1D). [c] Shoulder.

Table 5. AOM bonding and interelectronic Racah parameters (in cm^{-1}, rounded) for [(Tpms^{tBu})NiCl] (**2a**) and [(Tpms^{tBu})-CoCl(Hpz^{tBu})] (**3**) as obtained from the analysis of d−d transitions in the optical absorption spectra

	e_σ^{pz}	$e'_{\pi\perp}{}^{pz}$	e_σ^{Cl}	e_π^{Cl}	e_σ^{O}	e_π^{O}	B	*C*/*B*
2a	5400	400	4500	350	–	–	690	5.3
3	5300	800	4700	400	5800	1000	450	5.8

symmetry or any useful pseudo-symmetry. Moreover, since Tpms^{tBu} coordinates in the N,N,O mode, additional parameters for the Co−OSO$_2$ group have to be considered when applying the AOM. This situation demands substantial spectroscopic information, which is deduced, once more, from the low-temperature spectrum obtained from microcrystalline powders. As can been seen in Figure 6, the overall band pattern again is not changed, while the spectral resolution is largely improved on cooling down to T = 10 K.

To elucidate the complicated absorption structure, we proceeded as follows. First, we asked what would a simple electrostatic ligand field calculation, where all ligators are assumed to contribute by the same potential, predict for this particular geometry (Figure 5). It turns out that such a point charge approximation may already explain the overall band pattern. The present high-spin d^7 system exhibits a quartet ground term and nine more higher quartet states, which, unfortunately, cannot be related to parent states arising from any higher symmetric fivefold coordination. Under the reasonable assumption that the more intense transitions are due to spin-allowed transitions, we performed an optimization under the restrictions given above. This procedure results in a reasonable fit, whereby the expected quartet transition energies vary in the optical spectrum from 14000 to 20000 cm^{-1}, which is in line with the experimental findings. This result demonstrates that the geometrical structure of the chromophore is the main reason for the colour of **3**. In a second step, we have distinguished between σ- and π-bonding peculiarities and allowed free variation for the e_σ parameters involved. The AOM calculation then leads to a significantly better result, with the differences between calculated and observed spin-allowed transitions, obtained from a band deconvolution, becoming ca. 1000 cm^{-1} or less. The reliability of the subsequent assignments is confirmed by the parameter values derived from the fitting procedure, which show, for example, the expected trend for the σ donors: $e_\sigma^{O} > e_\sigma^{N} > e_\sigma^{Cl}$.[11]

Though keeping in mind the problem of overparametrization, a more-convincing band fit can be achieved when absorptions located around 18000 cm^{-1} are assigned to transitions into doublet states. Such spin-forbidden bands gain intensity by low symmetry and by the relatively large spin-orbit coupling present in cobalt(II) complexes. Under these assumptions, the AOM allows us to fit the absorption band pattern fairly well. It follows that the main peaks at 511, 597 and 633 nm represent quartet bands, whereby the latter broader bands cover two spin-allowed transitions each. All the other spectral features should arise from spin-forbidden transitions into doublet states. Spin-orbit coupling, however, mixes quartet and doublet states and causes further band shifts and level splittings.[15] Therefore, clear-cut assignments to be used in the optimization procedure cannot be made, which prevents the evaluation of definite AOM parameter values. In Table 5 we present an estimation only for the underlying model parameters. Nevertheless, it can certainly be concluded that the optical spectrum is due to metal-localized d−d transitions, which can be reasonably described by the AOM. We show that the distinct geometric arrangement of ligator atoms causes the specific spectral

pattern, rather then bonding peculiarities of the various ligating groups.

4. Zinc−Acetate Complexes of Tpms^{tBu}

Tl(Tpms^{tBu}) reacts with diethylzinc in tetrahydrofuran to give [(Tpms^{tBu})ZnEt] (**4**). The instability of ethylthallium leads to the precipitation of metallic thallium, which can be separated easily by centrifugation. The reaction of **4** with acetic acid yields acetato complexes. Varying the stoichiometric ratio results in two different products. With 1 equiv. of acetic acid, the expected acetato complex [(Tpms^{tBu})-ZnOAc] (**5a**) is formed. The reaction of **4** with 0.5 equiv. of acid, surprisingly, generates a dinuclear Tpms^{tBu} complex with a bridging acetato and a bridging hydroxo ligand (**5b**) (Scheme 2). The origin of the hydroxo ligand is unclear, it is probably due to traces of water in the solvent.

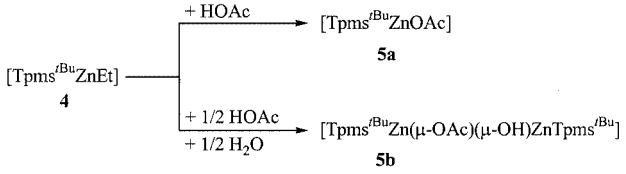

Scheme 2. Synthesis of the acetato complexes **5a** and **5b**

The complexes **5a** and **5b** can easily be distinguished spectroscopically. On the one hand, the intensity ratios of the pyrazolyl signals to the methyl signal of the acetato group in the ^{1}H NMR spectra are different. On the other hand, the OH valence stretching vibration of **5b** is clearly identified as a sharp band at 3620 cm^{-1} in the IR spectrum. It is a very sensitive probe for the non-associated OH group.

Table 6 displays the carboxylate stretching vibrations $\nu_{as}(CO_2)$ and $\nu_s(CO_2)$ of **5a** and **5b**. The position of $\nu_{as}(CO_2)$ and the difference $\Delta\nu(CO_2) = \nu_{as}(CO_2) - \nu_s(CO_2)$ are useful probes for determining the coordination mode of the acetato ligand.[16] The position of $\nu_{as}(CO_2)$ and the large value of $\Delta\nu(CO_2)$ in the case of **5a** indicates a monodentate coordination. This η^1-coordination was proven for [Tp^{tBu}ZnOAc] by Parkin through a crystal structure analysis[17] and is well known for other Tp^{R}Zn−carboxylato complexes.[9] The band for the asymmetric valence stretching $\nu_{as}(CO_2)$ of **5b** is shifted to smaller wavenumbers and the decrease of $\Delta\nu(CO_2)$ is typical for a bridging acetato ligand.[16]

Table 6. Carboxylate stretching vibrations (cm^{-1}) for **5a** and **5b** in the solid state

Compound	$\nu_{as}(CO_2)$	$\nu_s(CO_2)$	$\Delta\nu(CO_2)$
5a	1592	1331	261
5b	1573	1437	136

The crystal structure analysis of **5b** confirmed the spectroscopic results suggesting the bridging nature of the acetato and hydroxo ligands. Complex **5b** crystallises from diethyl ether in the monoclinic space group *I*2a, and the asymmetric unit of the crystal structure contains one molecule of diethyl ether. Figure 7 shows an ORTEP plot of **5b**. Selected bond lengths and angles are summarised in Table 7.

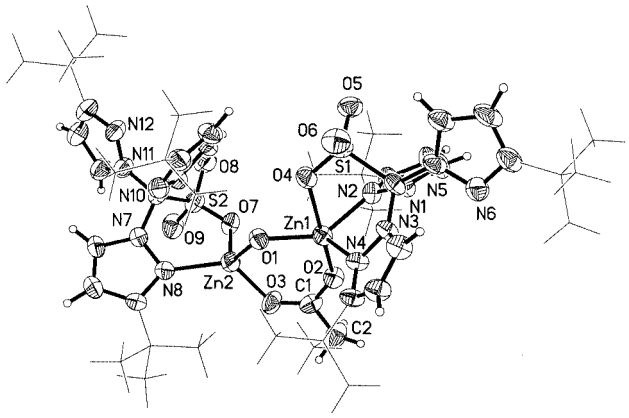

Figure 7. ORTEP plot of [(Tpms^{tBu})Zn(μ-OAc)(μ-OH)Zn-(Tpms^{tBu})] (**5b**)

Table 7. Selected bond lengths [Å] and angles [°] in [(Tpms^{tBu})Zn(μ-OAc)(μ-OH)Zn(Tpms^{tBu})] (**5b**)

Zn1−O1	1.938(3)	O1−Zn1−O2	95.74(12)
Zn1−O2	2.029(3)	O1−Zn1−N2	138.49(14)
Zn1−N2	2.064(4)	O2−Zn1−N2	94.64(14)
Zn1−N4	2.116(4)	O1−Zn1−N4	119.83(14)
Zn1−O4	2.273(3)	O2−Zn1−N4	107.16(13)
Zn2−O1	1.930(3)	N2−Zn1−N4	94.90(16)
Zn2−O3	1.939(3)	O1−Zn1−O4	82.19(11)
Zn2−O7	2.002(3)	O2−Zn1−O4	170.55(12)
Zn2−N8	2.053(4)	N2−Zn1−O4	81.13(13)
S1−O5	1.428(3)	N4−Zn1−O4	81.72(13)
S1−O6	1.442(3)	O1−Zn2−O3	101.98(13)
S1−O4	1.458(3)	O1−Zn2−O7	115.72(13)
S1−C3	1.888(5)	O3−Zn2−O7	98.45(14)
S2−O8	1.428(4)	O1−Zn2−N8	118.04(13)
S2−O9	1.437(3)	O3−Zn2−N8	126.15(16)
S2−O7	1.482(3)	O7−Zn2−N8	95.11(15)
S2−C25	1.861(5)	Zn2−O1−Zn1	123.12(14)
O2−C1	1.293(5)	O3−C1−O2	125.4(5)

It was surprising to us that the two zinc atoms have different coordination numbers in the solid state: four and five. One Tpms^{tBu} ligand coordinates in the known N,N,O mode, whereas the other acts as a bidentate N,O ligand. These different coordination modes are due to the asymmetrical bridge between the zinc atoms. Because of the short hydroxo bridge, the structure of **5b** is folded and the sterically demanding *tert*-butyl groups prevent the coordination of the second pyrazolyl ring.

NMR spectroscopic studies on **5b** ($CDCl_3$ and CD_2Cl_2) at room temperature show that all the pyrazole rings are equivalent in solution; i.e., the pyrazole rings undergo dynamic exchange. This exchange is fast on the NMR spectroscopic time scale, even at 203 K (CD_2Cl_2).

The dinuclear complex **5b** is an excellent structural model of dinuclear centres of the zinc enzymes phospholipase C and phosphotriesterase. Both of these enzymes contain a

dinuclear zinc centre with N,N,O binding motifs with the zinc ions connected by a bridging hydroxo and a bridging carboxylato ligand (phosphotriesterase: carbamylated lysin).[18] The Zn−Zn distance in the enzymes is 3.3 Å, which is nearly the same as in our model complex **5b** [Zn−Zn: 3.4008(8) Å].

5. Studies on Carbonylcopper(I) Complexes

To compare the donor abilities of Tpms^{tBu} with that of other tripodal ligands, we synthesised carbonylcopper(I) complexes. The CO stretching frequency strongly correlates with the electronic properties of the metal centre.

[(Tpms^{tBu})Cu(CO)] (**6a**) was obtained by the reaction of Tl(Tpms^{tBu}) and copper(I) chloride in dichloromethane under a carbon monoxide pressure of 3−4 bar. In addition, we synthesised [(Tpms)Cu(CO)] (**6b**) by the reaction of KTpms with a carbon monoxide saturated solution of [Cu(MeCN)$_4$]PF$_6$ in methanol. The IR spectra in dichloromethane (Figure 8) show that in solution both carbonyl complexes exist in two isomeric forms, like the zinc complexes **1a** and **1b** (Scheme 3)

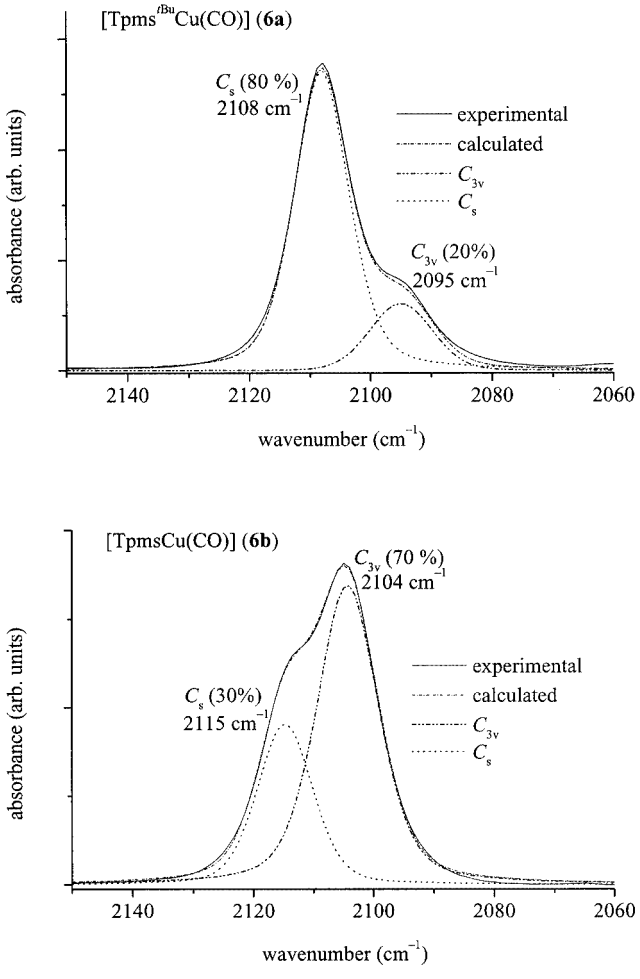

Figure 8. Analysis of the IR spectra (CO stretching bands) of the carbonyl complexes **6a** and **6b** in dichloromethane solution

From variable-temperature NMR spectroscopic studies we know that in the case of [(Tpms^{tBu})Cu(CO)] (**6a**) the C_s-symmetrical species is the preferred isomer, and, therefore, the more intense CO band (2108 cm^{-1}) is assigned to this isomer. [(Tpms)Cu(CO)] (**6b**) favours the N,N,N coordination mode in solution, and, therefore, the more intense CO band (2104 cm^{-1}) is assigned to the C_{3v}-symmetrical complex. The different behaviour of the Tpms^{tBu} ligand, compared to the Tpms one, may be a consequence of the repulsion between the *tert*-butyl groups and the carbonyl ligand.

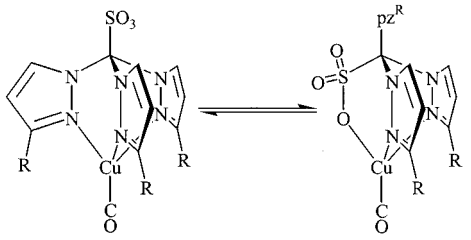

Scheme 3. Equilibrium between the N,N,N mode (C_{3v}) and the N,N,O mode (C_s) (R = H, *t*Bu)

Table 8 displays a comparison of CO stretching vibrations of tripodal nitrogen ligand complexes of the type [(ligand)Cu(CO)].

Table 8. CO stretching vibrations (cm^{-1}) of carbonylcopper(I) complexes of the type [(ligand)Cu(CO)] in the solid state

Ligand	ν(CO)	Ligand	ν(CO)	Ligand	ν(CO)
Tpms	2101	Tp	2083[a] [23]	HC(pz^{Me,Me})$_3$	2113[24]
Tpms^{tBu}	2093/2088	Tp^{tBu}	2069[25]	HC(pz^{tBu})$_3$	2100[24]
		Tp^{Me,Me}	2060[26]		
		Tp^{iPr,iPr}	2056[27]		

[a] In light petroleum ether.

In the Tp complexes, the CO stretching vibrations are shifted towards lower energies compared to those of **6a** and **6b**. Thus, the Tpms ligands are weaker donors than the Tp ligands. The anionic Tpms ligands are stronger donors compared to the neutral tris(pyrazolyl)methane ligands.

From the IR spectra measured in the temperature range from −10 to +83 °C, we have determined the equilibrium constants for the two isomeric forms of [(Tpms^{tBu})Cu(CO)] (**6a**) in toluene. With a van't Hoff plot we calculated the enthalpy and entropy of the transformation of the C_{3v}-symmetrical species into the C_s-symmetrical one. The resulting values are $\Delta H = +6$ kJ·mol^{-1} and $\Delta S = +35$ J·K^{-1}·mol^{-1}. Variable-temperature ^{1}H NMR measurements in CD_2Cl_2 (−70 to +5 °C) yield the same values. They are very similar to the thermodynamic parameters of [(Tpms^{tBu})ZnCl] (**1a**) (see above).

Conclusion

The thallium salt of the sterically demanding ligand Tpms^{tBu} is a convenient starting material for halide com-

plexes of zinc(II), nickel(II) and cobalt(II) ions, as well as for alkylzinc and carbonylcopper(I) complexes. Tpms^{tBu} can act as a tripodal N,N,N ligand, as a tripodal N,N,O ligand and as a bipodal N,O ligand. In Rh^{I} complexes, we have observed Tpms to exhibit bipodal N,N coordination.[7] From the CO stretching vibrations of **6a** and **6b** we conclude that the tripodal Tpms ligands are weaker donors than are tris(-pyrazolyl)borate ligands. The equilibrium between C_{3v}- and C_s-symmetrical complexes in solution (**1a**, **1b**, **6a**, **6b**) indicates that, in the solvents that we have used here, there is no significant difference in the stabilities of the N,N,N and the N,N,O coordination modes. The equilibration between the two isomeric forms is slow on the NMR spectroscopic time scale. The formation of **3** shows that hydrolysis of the Tpms^{tBu} ligand occurs in the presence of certain metal ions; we have not yet observed this behaviour with the unsubstituted Tpms ligand. The coordination number of the Tpms complexes is not restricted to four. In the sterically less demanding N,N,O coordination mode the ligand allows also a coordination number of five (**3**, **5b**). All in all, this feature demonstrates that Tpms^{tBu} is a structurally flexible ligand that can adapt to the preferences of the metal centre. The complexes described here are soluble in polar solvents, like wet methanol. This solubility should allow reactivity studies of metalloenzyme model compounds with Tpms ligands to be carried out under more realistic conditions than with model compounds containing the highly hydrophobic Tp ligands.

Experimental Section

General Remarks: The compound KTpms was synthesised according to a published procedure.[1] All other reagents were commercial samples and were used as received. All reactions were carried out under nitrogen using standard Schlenk techniques, unless stated otherwise. Solvents were purified and degassed by standard procedures. Filtration was carried out using 1-μm membrane filters (regenerated cellulose, Schleicher & Schuell). Centrifugation was carried out using a Hettich Rotina 46 Schlenk tube centrifuge. ^1H and ^{13}C NMR spectra were recorded with Bruker DRX 200 (at 293 K) or Bruker DRX 500 (at 298 K) spectrometers. Chemical shifts (δ) are given in ppm referenced to the solvent peak.[19] Infrared spectra were recorded with a Bruker IFS 66 FT spectrometer. FAB mass spectra were recorded with a Finnigan MAT 8200 instrument (Ar, 8 kV, matrix: NBA unless stated otherwise). Elemental analyses were performed with a Perkin−Elmer CHN-2400/II elemental analyser. The absorption spectra of **2a** and **3**, dissolved in dichloromethane, were recorded with a Analytik Jena Specord S 100 spectrometer. Microcrystalline powders of both compounds were embedded in polyethylene pellets and their transmission was measured with a Cary 4 spectrometer. Temperatures down to 10 K were achieved by using a commercial flow-cryostat technique.

Tl(Tpms^{tBu}): Under cooling to −65 °C, a solution of *n*-butyllithium (1.6 M, 42 mL) was added to a solution of tris(3-*tert*-butylpyrazolyl)methane[20] (21 g, 54 mmol) in diethyl ether (60 mL). The solution immediately turned red and later became brown. After 40 min, sulfur trioxide−trimethylamine complex (8.4 g, 60 mmol) was added at −35 °C. Under constant stirring, the resulting suspension was warmed to room temperature overnight. The solvent was then evaporated. To remove excess tris(3-*tert*-butylpyrazolyl)methane, the residue was treated with dichloromethane, stirred for 1 h, filtered and washed with pentane, to yield an off-white powder (15 g). Recrystallisation from boiling toluene (400 mL) yielded colourless crystals of Li(Tpms^{tBu}) (8.9 g, 19 mmol, 36%). The thallium salt was obtained by adding a solution of $TlNO_3$ (10 g, 37 mmol) in a methanol/water mixture (3:7, 100 mL) to a solution of Li(Tpms^{tBu}) (8.9 g, 19 mmol) in a methanol/water mixture (7:3, 100 mL) in a beaker. Tl(Tpms^{tBu}) precipitated as a white solid. The precipitate was washed with water and dried under reduced pressure at room temperature. Yield: 8.6 g, 68%. ^1H NMR (200 MHz, $CDCl_3$): δ = 1.31 (s, 27 H, CH_3), 6.27 (d, $^3J_{H,H}$ = 2.7 Hz, 3 H, pyrazolyl 4-*H*), 7.43 (d, $^3J_{H,H}$ = 2.7 Hz, 3 H, pyrazolyl 5-*H*) ppm. $^{13}C\{^1H\}$ NMR (500 MHz, $CDCl_3$): δ = 31.4 [s, C(*C*H_3)$_3$], 33.1 [s, (CH$_3$)$_3$*C*], 97.1 (s, *C*SO_3), 105.2 (s, pyrazolyl *C*-4), 134.3 (s, pyrazolyl *C*-5), 165.2 (s, pyrazolyl *C*-3) ppm. IR (KBr): $\tilde{\nu}$ = 3155, 3124 [w, ν(C−H)], 2959 [vs, ν(C−H), CH_3], 1530 [m, ν(C=C)], 1481, 1463 [m, δ_{as}(*t*Bu)], 1397, 1363 [vs, δ_s(*t*Bu)], 1033 [(vs, ν_s(SO)], 636 [s, ν(C−S] cm^{-1}. MS (FAB$^+$): *m*/*z* = 871 [M + Tl]$^+$, 667 [M + H]$^+$, 381 [M − SO_3Tl]$^+$. $C_{22}H_{33}N_6O_3STl$ (665.99): calcd. C 39.7, H 5.0, N 12.6; found C 39.7, H 4.9, N 12.7.

[(Tpms^{tBu})MX] Complexes: The preparation of [(Tpms^{tBu})ZnCl] (**1a**) is described in detail as a representative example of this type of complex. Workup procedures and spectroscopic data for the analogous complexes are described below.

[(Tpms^{tBu})ZnCl] (1a): A stirred solution of Tl(Tpms^{tBu}) (0.92 g, 1.4 mmol) in methanol (20 mL) was treated with $ZnCl_2$ (0.19 g, 1.4 mmol) at room temperature. After 1 h of stirring, the precipitated TlCl was filtered and the solvent was evaporated under reduced pressure. The colourless residue was dissolved in a small amount of dichloromethane, filtered and the product was precipitated with pentane. The white powder was washed with pentane and dried at 40 °C for 24 h under reduced pressure (yield: 0.54 g, 70%). ***C*$_s$-Symmetrical Complex:** ^1H NMR (200 MHz, $CDCl_3$): δ = 1.46 (s, 9 H, CH_3), 1.51 (s, 18 H, CH_3), 6.36 (d, $^3J_{H,H}$ = 2.8 Hz, 2 H, pyrazolyl 4-*H*), 6.49 (d, $^3J_{H,H}$ = 2.5 Hz, 1 H, pyrazolyl 4-*H*), 6.85 (d, $^3J_{H,H}$ = 2.8 Hz, 2 H, pyrazolyl 5-*H*), 8.78 (d, $^3J_{H,H}$ = 2.5 Hz, 1 H, pyrazolyl 5-*H*) ppm. ***C*$_{3v}$-Symmetrical Complex:** ^1H NMR (200 MHz, $CDCl_3$): δ = 1.34 (s, 27 H, CH_3), 6.32 (d, $^3J_{H,H}$ = 3.0 Hz, 3 H, pyrazolyl 4-*H*), 9.07 (d, $^3J_{H,H}$ = 3.0 Hz, 3 H, pyrazolyl 5-*H*) ppm; ratio C_s:C_{3v} = 3.4:1. $^{13}C\{^1H\}$ NMR (500 MHz, CD_2Cl_2): δ = 30.0, 30.1, 30.3 [s, C(*C*H$_3$)$_3$], 32.6, 32.7, 32.9 [s, *C*(CH$_3$)$_3$], 94.5 (s, *C*SO_3), 104.3, 105.1, 106.3 (s, pyrazolyl *C*-4), 136.1, 136.5, 137.2 (s, pyrazolyl *C*-5), 167.3, 168.2 (s, pyrazolyl *C*-3) ppm. IR (KBr): $\tilde{\nu}$ = 3163 [w, ν(C−H)], 2969 [vs, ν(C−H)], CH_3], 1526 [m, ν(C=C)], 1401, 1368[vs, δ_s(*t*Bu)], 1036[vs, ν_s(SO)], 652[vs, ν(C−S)] cm^{-1}. MS (FAB$^+$): *m*/*z* = 561 [M + H]$^+$, 525 [M − Cl]$^+$, 463 [Tpms^{tBu} + 2H]$^+$, 381 [C(pz^{tBu})$_3$]$^+$, 259 [C(pz^{tBu})$_2$ + H]$^+$, 57 [*t*Bu]$^+$. $C_{22}H_{33}ClN_6O_3SZn$ (562.45): calcd. C 47.0, H 5.9, N 14.9, found C 47.4, H 6.2, N 14.3.

[(Tpms^{tBu})ZnBr] (1b): $ZnBr_2$ (0.16 g, 0.73 mmol), Tl(Tpms^{tBu}) (0.47 g, 0.71 mmol), yield: 0.28 g (65%) of a white powder. Crystals suitable for X-ray analysis were obtained by diffusion of pentane in a concentrated solution of **1b** in THF. ***C*$_s$-Symmetrical Complex:** ^1H NMR (200 MHz, $CDCl_3$): δ = 1.35 (s, 9 H, CH_3), 1.53 (s, 18 H, CH_3), 6.36 (d, $^3J_{H,H}$ = 3.0 Hz, 2 H, pyrazolyl 4-*H*), 6.50 (d, $^3J_{H,H}$ = 2.7 Hz, 1 H, pyrazolyl 4-*H*), 6.84 (d, $^3J_{H,H}$ = 3.0 Hz, 2 H, pyrazolyl 5-*H*), 8.79 (d, $^3J_{H,H}$ = 2.7 Hz, 1 H, pyrazolyl 5-*H*) ppm. ***C*$_{3v}$-Symmetrical Complex:** ^1H NMR (200 MHz, $CDCl_3$): δ = 1.48 (s, 27 H, CH_3), 6.33 (d, $^3J_{H,H}$ = 3.1 Hz, 3 H, pyrazolyl 4-*H*), 9.09 (d, $^3J_{H,H}$ = 3.1 Hz, 3 H, pyrazolyl 5-*H*) ppm; ratio C_s/C_{3v} = 10:1. $^{13}C\{^1H\}$ NMR (500 MHz, CD_2Cl_2): δ = 30.0, 30.5 [s, C(*C*H$_3$)$_3$],

32.9 [s, $C(CH_3)_3$], 94.5 (s, CSO_3), 104.5, 105.2, 106.3 (s, pyrazolyl *C*-4), 136.2, 136.5, 137.2 (s, pyrazolyl *C*-5), 167.4, 168.2 (s, pyrazolyl *C*-3) ppm. IR (KBr): $\tilde{\nu}$ = 3163 [w, ν(C−H)], 2969 [vs, ν(C−H), CH_3], 1525 [m, ν(C=C)], 1401, 1369 [vs, δ_s(*t*Bu)], 1036 [vs, ν_s(SO)], 652 [vs, ν(C−S)] cm^{-1}. MS (FAB^+): *m*/*z* = 607 $[M + H]^+$, 525 $[M - Br]^+$, 463 $[(Tpms^{tBu}) + 2\ H]^+$, 381 $[C(pz^{tBu})_3]^+$, 259 $[C(pz^{tBu})_2 + H]^+$, 57 $[tBu]^+$. $C_{22}H_{33}BrN_6O_3SZn$ (606.90): calcd. C 43.5, H 5.5, N 13.8, found C 43.7, H 5.6, N 13.4.

[(Tpms^{tBu})ZnI] (1c): ZnI_2 (0.29 g, 0.91 mmol), Tl(Tpms^{tBu}) (0.61 g, 0.91 mmol), yield: 0.36 g (52%) of a white powder. ^1H NMR (200 MHz, $CDCl_3$): δ = 1.34 (s, 9 H, C*H*$_3$), 1.56 (s, 18 H, C*H*$_3$), 6.35 (d, $^3J_{H,H}$ = 2.7 Hz, 2 H, pyrazolyl 4-*H*), 6.49 (br. s, 1 H, pyrazolyl 4-*H*), 6.83 (d, $^3J_{H,H}$ = 2.7 Hz, 2 H, pyrazolyl 5-*H*), 8.80 (br. s, 1 H, pyrazolyl 5-*H*) ppm. $^{13}C\{^1H\}$ NMR (500 MHz, CD_2Cl_2): δ = 30.2, 31.0 [s, C(*C*H$_3$)$_3$], 32.9 [s, *C*(CH$_3$)$_3$], 94.5 (s, *C*SO$_3$), 105.3, 106.2 (s, pyrazolyl *C*-4), 136.2 (s, pyrazolyl -*C*5), 167.6, 168.3 (s, pyrazolyl *C*-3) ppm. IR (KBr): $\tilde{\nu}$ = 3163 [w, ν(C−H)], 2969 [vs, ν(C−H), CH_3], 1525 [m, ν(C=C)], 1400, 1369 [vs, δ_s(*t*Bu)], 1035 [vs, ν_s(SO)], 652 [vs, ν(C−S)] cm^{-1}. MS (FAB^+): *m*/*z* = 653 $[M + H]^+$, 525 $[M - I]^+$, 515 $[M - SO_3 - tBu]$, 381 $[C(pz^{tBu})_3]^+$, 259 $[C(pz^{tBu})_2 + H]^+$, 57 $[tBu]^+$. $C_{22}H_{33}IN_6O_3SZn\cdot 1/2CH_2Cl_2$ (696.37): calcd. C 38.8, H 4.9, N 12.1, found C 39.0, H 5.0, N 12.3.

[(Tpms^{tBu})NiCl] (2a): $NiCl_2\cdot 6H_2O$ (0.23 g, 0.97 mmol), Tl(Tpms^{tBu}) (0.64 g, 0.96 mmol). Diffusion of pentane into a concentrated solution of the crude product in THF yielded dark red crystals (0.13 g, 25%) suitable for X-ray analysis. IR (KBr): $\tilde{\nu}$ = 3169 [w, ν(C−H)], 2975 [vs, ν(C−H), CH_3], 1527 [m, ν(C=C)], 1397, 1364 [vs, δ_s(*t*Bu)], 1055 [vs, ν_s(SO)], 619 [s, ν(C−S)] cm^{-1}. MS (FAB^+): *m*/*z* = 643 $[M - Cl + Hpz^{tBu}]^+$, 519 $[M - Cl]^+$, 463 $[M - Cl - SO_3]^+$, 381 $[C(pz^{tBu})_3]^+$, 259 $[C(pz^{tBu})_2 + H]^+$. UV/Vis (CH_2Cl_2): λ_{max} (ε_{max}) = 475 nm (370 $M^{-1}\cdot cm^{-1}$). $C_{22}H_{33}ClN_6NiO_3S$ (555.75): calcd. C 47.6, H 6.0, N 15.1, found C 47.6, H 5.8, N 15.3.

[(Tpms^{tBu})NiBr] (2b): $NiBr_2\cdot 3H_2O$ (0.08 g, 0.29 mmol), Tl(Tpms^{tBu}) (0.19 g, 0.29 mmol). Diffusion of pentane into a concentrated THF solution of the crude product yielded red crystals (0.03 g, 17%). IR (KBr): $\tilde{\nu}$ = 3156 [(w, ν(C−H)], 2969 [vs, ν(C−H), CH_3], 1526 [m, ν(C=C)], 1400, 1368 [vs, δ_s(*t*Bu)], 1030 [vs, ν_s(SO)], 619 [s, ν(C−S)] cm^{-1}. MS (FAB^+): *m*/*z* = 643 $[M - Br + Hpz^{tBu}]^+$, 519 $[M - Br]^+$, 463 $[M - Br - SO_3]^+$, 381 $[C(pz^{tBu})_3]^+$, 259 $[C(pz^{tBu})_2 + H]^+$. UV/Vis (CH_2Cl_2): λ_{max} (ε_{max}) = 485 nm (450 $M^{-1}\cdot cm^{-1}$). $C_{22}H_{33}BrN_6NiO_3S\cdot 1/2C_4H_8O$ (636.26): calcd. C 45.3, H 5.9, N 13.2, found C 45.1, H 6.0, N 13.1.

[(Tpms^{tBu})CoCl(Hpz^{tBu})] (3): A stirred solution of $CoCl_2$ (0.16 g, 1.2 mmol) (dried at 150 °C under reduced pressure for 8 h) in methanol (5 mL) was treated with a solution of Tl(Tpms^{tBu}) (0.67 g, 1.0 mmol) in methanol (15 mL) at room temperature. The precipitated TlCl was separated after 15 min and the solvent was evaporated under reduced pressure. The blue residue was dissolved in dichloromethane (10 mL) and the solution was filtered. Evaporation of the solvent and then washing the residue with pentane yielded a blue powder (0.45 g, 0.66 mmol, 55%). Analytically pure crystals suitable for X-ray analysis were obtained by diffusion of pentane into a concentrated solution of **3** in THF. Yield: 0.18 g (24%). UV/Vis (CH_2Cl_2): λ_{max} (ε_{max}) = 520 nm (167 $M^{-1}\cdot cm^{-1}$), 558 (214), 603 (402), 674 (48). IR (KBr): $\tilde{\nu}$ = 3380 [s, ν(N−H)], 3159 [w, ν(C−H)], 2965 [vs, ν(C−H), CH_3], 1530 [s, ν(C=C)], 1397, 1365 [s, δ_s(*t*Bu)], 1042 [s, ν_s(SO)], 644 [s, ν(C−S)] cm^{-1}. MS (FAB^+): *m*/*z* = 644 $[M - Cl]^+$, 520 $[M - Cl - Hpz^{tBu}]^+$, 440 $[M - Cl - Hpz^{tBu} - SO_3]^+$, 381 $[C(pz^{tBu})_3]^+$, 259 $[C(pz^{tBu})_2 + H]^+$. $C_{29}H_{45}ClCoN_8O_3S\cdot C_4H_8O$ (752.29): calcd. C 52.7, H 7.1, N 14.9, found C 51.7, H 7.0, N 14.6.

[(Tpms^{tBu})ZnEt] (4): A solution of Tl(Tpms^{tBu}) (1.7 g, 2.5 mmol) in THF (30 mL) was added dropwise at room temperature to a solution of $ZnEt_2$ (1 M solution in hexane, 3.0 mL, 3.0 mmol) in THF (20 mL). The precipitated thallium metal was separated by centrifugation. The colourless supernatant solution was concentrated until the onset of crystallisation and then left to stand at −30 °C. After 2 d, colourless crystals (1.0 g, 64%) were collected by filtration. ^1H NMR (200 MHz, C_6D_6): δ = 1.00 (q, $^3J_{H,H}$ = 8.0 Hz, 2 H, C*H*$_2$), 1.15 [s, 27 H, C(C*H*$_3$)$_3$], 1.72 (t, $^3J_{H,H}$ = 8.0 Hz, 3 H, C*H*$_3$), 5.73 (br. s, 2 H, pyrazolyl 4-*H*), 5.94 (br. s, 1 H, pyrazolyl 4-*H*), 6.74 (br. s, 2 H, pyrazolyl 5-*H*), 9.24 (br. s, 1 H, pyrazolyl 5-*H*) ppm. $^{13}C\{^1H\}$ NMR (500 MHz, C_6D_6): δ = 5.6 (s, *C*H$_2$CH$_3$), 12.7 (s, CH$_2$*C*H$_3$), 30.8, 31.0 [s, C(*C*H$_3$)$_3$], 32.9, 33.3 [s, *C*(CH$_3$)$_3$], 95.4 (s, *C*SO$_3$), 104.7, 106.0 (s, pyrazolyl *C*-4), 135.8, 137.9 (s, pyrazolyl *C*-5), 166.9 (s, pyrazolyl *C*-3) ppm. IR (KBr): $\tilde{\nu}$ = 3163 [w, ν(C−H)], 2964 [vs, ν(C−H), CH_3], 1524 [s, ν(C=C)], 1399, 1367 [vs, δ_s(*t*Bu)], 1043 [vs, ν_s(SO)], 649 [vs, ν(C−S)] cm^{-1}. MS (FAB^+; matrix: NPOE): *m*/*z* = 649 $[M - Et + Hpz^{tBu}]^+$, 555 $[M + H]^+$, 525 $[M - Et]^+$, 445 $[M - SO_3 - tBu]$, 381 $[C(pz^{tBu})_3]^+$, 57 $[tBu]^+$. $C_{24}H_{38}N_6O_3SZn\cdot C_4H_8O$ (628.17): calcd. C 53.5, H 7.4, N 13.4, found C 53.1, H 7.5, N 13.5.

[(Tpms^{tBu})ZnOAc] (5a): A solution of **4** (0.61 g, 0.97 mmol) in THF (10 mL) was treated with acetic acid (55 μL, 0.97 mmol). After 10 min of stirring at room temperature, the solution was concentrated under reduced pressure and the product was precipitated with hexane. Yield: 0.11 g (20%) of a white powder. ^1H NMR (200 MHz, C_6D_6): δ = 1.24 [s, 27 H, C(C*H*$_3$)$_3$], 1.96 (s, 3 H, acetate C*H*$_3$), 5.89 (d, $^3J_{H,H}$ = 2.8 Hz, 3 H, pyrazolyl 4-*H*) 7.66 (br. s, 3 H, pyrazolyl 5-*H*) ppm. $^{13}C\{^1H\}$ NMR (500 MHz, C_6D_6): δ = 23.7 (s, *C*H$_3$CO$_2$), 30.8 [s, C(*C*H$_3$)$_3$], 33.2 [s, *C*(CH$_3$)$_3$], 96.6 (s, *C*SO$_3$), 105.8 (s, pyrazolyl *C*-4), 136.3 (s, pyrazolyl *C*-5), 166.7 (s, pyrazolyl *C*-3), 182.3 (s, CH$_3$*C*O$_2$) ppm. IR (KBr): $\tilde{\nu}$ = 3126 [w, ν(C−H)], 2966 [vs, ν(C−H), CH_3], 1592 [vs, $\nu_{as}(CO_2)$], 1532 [s, ν(C=C)], 1403, 1366 [s, δ_s(*t*Bu)], 1331 [s, $\nu_{as}(CO_2)$], 1036 [vs, ν_s(SO)], 647 [vs, ν(C−S)] cm^{-1}. MS (FAB^+): *m*/*z* = 381 $[C(pz^{tBu})_3]^+$, 259 $[C(pz^{tBu})_2 + H]^+$, 57 $[tBu]^+$. $C_{24}H_{36}N_6O_5SZn$ (586.04): calcd. C 49.2, H 6.2, N 14.3, found C 49.1, H 6.3, N 14.1.

[(Tpms^{tBu})Zn(μ-OAc)(μ-OH)Zn(Tpms^{tBu})] (5b): A solution of **4** (0.32 g, 0.51 mmol) in benzene (5 mL) was treated with acetic acid (19 μL, 0.34 mmol). After 10 min of stirring at room temperature, the solvent was evaporated under reduced pressure. The residue was treated with a small amount of diethyl ether and filtered, and then the colourless solution was stored at −30 °C overnight. Analytically pure crystals suitable for X-ray analysis were collected by filtration. Yield: 0.05 g (16%). ^1H NMR (200 MHz, $CDCl_3$): δ = 1.33 [s, 54 H, C(C*H*$_3$)$_3$], 2.02 (s, 3 H, acetate C*H*$_3$), 6.34 (d, $^3J_{H,H}$ = 2.9 Hz, 6 H, pyrazolyl 4-*H*), 7.45 (d, $^3J_{H,H}$ = 2.9 Hz, 6 H, pyrazolyl 5-*H*) ppm. $^{13}C\{^1H\}$ NMR (500 MHz, CD_2Cl_2): δ = 25.1 (s, *C*H$_3$CO$_2$), 30.3 [s, C(*C*H$_3$)$_3$], 32.6 [s, *C*(CH$_3$)$_3$], 95.3 (s, *C*SO$_3$), 105.5 (s, pyrazolyl *C*-4), 135.1 (s, pyrazolyl *C*-5), 166.6 (s, pyrazolyl *C*-3), 181.3 (s, CH$_3$*C*O$_2$) ppm. IR (KBr): $\tilde{\nu}$ = 3619 [m, sharp, ν(O−H)], 3155 [w, ν(C−H)], 2966 [vs, ν(C−H), CH_3], 1573 [vs, $\nu_{as}(CO_2)$], 1531 [s, ν(C=C)], 1437 [m, $\nu_{as}(CO_2)$], 1401, 1365 [s, δ_s(*t*Bu)], 1050 [s, ν_s(SO)], 646 [s, ν(C−S)] cm^{-1}. MS (FAB^+): *m*/*z* = 381 $[C(pz^{tBu})_3]^+$, 259 $[C(pz^{tBu})_2 + H]^+$. $C_{46}H_{70}N_{12}O_9S_2Zn_2\cdot C_4H_{10}O$ (1204.17): calcd. C 49.9, H 6.7, N 14.0, found C 49.9, H 6.7, N 13.9.

[(Tpms^{tBu})Cu(CO)] (6a): A solution of Tl(Tpms^{tBu}) (0.35 g, 0.52 mmol) in dichloromethane (5 mL) was saturated with carbon monoxide in a Schlenk tube equipped with a Teflon seal and valve. After 10 min, CuCl (0.10 g, 1.0 mmol) was added, the suspension was pressurized with 3−4 bar of carbon monoxide and stirred for 48 h at room temperature. Thereafter, the precipitated TlCl and

remaining CuCl was filtered off and the product was precipitated with hexane under carbon monoxide. The colourless product was isolated by filtration and washed with pentane. Yield: 0.14 g (50%). ^{1}H NMR (200 MHz, $CDCl_3$): δ = 1.33 (s, 9 H, C*H*$_3$), 1.49 (s, 18 H, C*H*$_3$), 6.25 (br. s, 2 H, pyrazolyl 4-*H*), 6.39 (br. s, 1 H, pyrazolyl 4-*H*), 6.74 (br. s, 2 H, pyrazolyl 5-*H*), 8.87 (br. s, 1 H, pyrazolyl 5-*H*) ppm. IR (KBr): $\tilde{\nu}$ = 3177, 3136 [w, ν(C−H)], 2972 [vs, ν(C−H), CH_3], 2093/2088 [vs, ν(CO)], 1528 [s, ν(C=C)], 1483, 1458 [m, δ_{as}(*t*Bu)], 1390, 1365 [s, δ_s(*t*Bu)], 1053 [vs, ν_s(SO)], 621 [vs, ν(C−S)] cm^{-1}. MS (FAB$^+$): *m*/*z* = 525 [M − CO + H]$^+$, 445 [M − SO_3 − CO + H]$^+$, 387 [M − SO_3 − CO − *t*Bu]$^+$, 381 [C(pz$^{t\mathrm{Bu}}$)$_3$]$^+$, 321 [M − SO_3 − CO − pz$^{t\mathrm{Bu}}$]$^+$, 57 [*t*Bu]$^+$. $C_{23}H_{33}CuN_6O_4S$ (553.17): calcd. C 49.9, H 6.0, N 15.2, found C 49.8, H 5.8, N 15.4.

[(Tpms)Cu(CO)] (6b): [Cu(MeCN)$_4$]PF_6 (259 mg, 0.7 mmol) was dissolved in methanol (10 mL). The colourless solution was saturated with carbon monoxide, stirred at room temperature for 20 min and then KTpms (229 mg, 0.7 mmol) was added. A white precipitate had formed within seconds. The mixture was stirred under CO for 1 h and then the precipitate was filtered off, washed with a small portion of methanol and dried for 4 h in a stream of dry N_2. Yield: 0.09 g (34%). ^{1}H NMR (200 MHz, CD_2Cl_2): δ = 6.41 (dd, $^3J_{H,H}$ = 1.7, 2.8 Hz, 3 H, pyrazolyl 4-*H*), 7.81 (d, $^3J_{H,H}$ = 1.7 Hz, 3 H, pyrazolyl 3-*H*), 8.45 (br. s, 3 H, pyrazolyl 5-*H*) ppm. ***C*$_s$-Symmetrical Complex:** ^{1}H NMR ($CDCl_3$, 200 MHz, 213 K) δ = 6.50 (dd, $^3J_{H,H}$ = 2.0, 2.6 Hz, 2 H, pyrazolyl 4-*H*), 6.64 (dd, $^3J_{H,H}$ = 1.9, 2.1 Hz, 1 H, pyrazolyl 4-*H*), 6.88 (d, $^3J_{H,H}$ = 2.6 Hz, 2 H, pyrazolyl 5-*H*), 7.91 (s, 2 H, pyrazolyl 3-*H*), 7.99 (s, 1 H, pyrazolyl 3-*H*), 8.9 (overlapped, 3 H, pyrazolyl 5-*H*) ppm. ***C*$_{3v}$-Symmetrical Complex:** ^{1}H NMR (200 MHz, $CDCl_3$): δ = 6.39 (dd, $^3J_{H,H}$ = 1.7, 2.8 Hz, 3 H, pyrazolyl 4-*H*), 7.75 (d, $^3J_{H,H}$ = 1.7 Hz, 3 H, pyrazolyl 3-*H*), 8.90 (d, $^3J_{H,H}$ = 2.8 Hz, 3 H, pyrazolyl 5-*H*) ppm; ratio C_s/C_{3v} = 1:3. IR (KBr): $\tilde{\nu}$ = 3180, 3127 [s, ν(C−H)], 2101 [vs, ν(CO)], 1524 [s, ν(C=C)], 1052 [vs, ν_s(SO)], 621 [vs, ν(C−S)] cm^{-1}. $C_{11}H_9CuN_6O_4S$ (384.84): calcd. C 34.3, H 2.4, N 21.8, found C 34.2, H 2.4, N 22.0.

X-ray Crystallographic Study: Crystals of compounds **1b**, **2a**, **3** and **5b** suitable for X-ray study were investigated with area-detector diffractometers using graphite-monochromated Mo-K_α radiation (λ = 0.71073 Å). Unit cell parameters were determined by least-squares refinements on the positions of 18000, 1953, 7998 and 2000 reflections in the range 2° < θ < 30.5°, 3° < θ < 27.5°, 2° < θ < 25° and 2° < θ < 25°, respectively. Space groups of type no. 14 were uniquely determined in the cases of **1b**, **2a** and **3**. In the case of **5b**, systematic extinctions were consistent with space groups *Ia* and *I*2/*a*, but the latter proved to be the correct one in the course of structure refinement. Lp corrections were applied to all the intensity data. In the case of **1b**, empirical absorption corrections have been performed ($T_{min.}$ = 0.175; $T_{max.}$ = 0.250), and in the case of **2a**, an empirical extinction parameter was refined. The structures were solved by direct methods[21] and the positions of all hydrogen atoms were found in the case of **1b**, **2a** and **5b**. In the case of **3**, the hydrogen atom positions of the tetrahydrofuran molecule were calcu-

Table 9. Crystallographic data for compounds **1b**, **2a**, **3** and **5b**

	1b	**2a**	**3**	**5b**
Empirical formula	$C_{48}H_{74}Br_2N_{12}O_7S_2Zn_2$	$C_{22}H_{33}ClN_6NiO_3S$	$C_{33}H_{25}ClCoN_8O_4S$	$C_{50}H_{79}N_{12}O_{10}S_2Zn_2$
Molecular mass	1285.87	555.76	751.27	1203.11
Crystal system	monoclinic	monoclinic	monoclinic	monoclinic
Space group	$P2_1/c$	$P2_1/n$	$P2_1/n$	$I2/a$
a [Å]	20.2171(3)	9.775(2)	12.010(2)	30.245(2)
b [Å]	15.6790(2)	17.935(4)	19.330(4)	11.0222(5)
c [Å]	21.0561(3)	15.186(3)	16.920(3)	38.801(3)
β [°]	115.8650(10)	95.67(3)	90.50(3)	98.508(10)
V [Å^3]	6005.83(15)	2649.3(9)	3927.9(13)	12792.6(14)
Z	4	4	4	8
F(000)	2656	1168	1592	5080
$D_{calcd.}$ [Mg·m^{-3}]	1.422	1.393	1.270	1.249
μ(Mo-K_α) [mm^{-1}]	2.254	0.946	0.603	0.874
Crystal size [mm]	0.45 × 0.40 × 0.25	0.51 × 0.34 × 0.33	0.30 × 0.25 × 0.20	0.72 × 0.33 × 0.28
Diffractometer	Bruker SMART CCD	Stoe IPDS	Stoe IPDS	Stoe IPDS
Monochromator	graphite	graphite	graphite	graphite
T [K]	173(2)	293(2)	293(2)	293(2)
Data-collecting mode	Ω scans	Φ scans	Φ scans	Φ scans
θ range [°]	1.12−30.46	2.27−27.50	2.00−25.01	1.85−25.00
hkl ranges	−28 ≤ *h* ≤ 16	−12 ≤ *h* ≤ 12	−14 ≤ *h* ≤ 14	−35 ≤ *h* ≤ 35
	−21 ≤ *k* ≤ 20	−23 ≤ *k* ≤ 23	−22 ≤ *k* ≤ 22	−13 ≤ k ≤ 13
	−28 ≤ *l* ≤ 28	−19 ≤ *l* ≤ 19	−20 ≤ *l* ≤ 20	−46 ≤ l ≤ 46
No. of reflns. measd.	46966	33151	43565	81477
No. of unique reflns.	16305	6031	6925	11243
No. of reflns. obsd. [$I > 2\sigma(I)$]	10093	5275	4754	3772
No. of param./restraints	925/0	317/0	481/0	706/0
Refinement method	Full-matrix least squares on F^2	Full-matrix least squares on F^2	Full-matrix least squares on F^2	Full-matrix least squares on F^2
Final *R* indices [$I > 2\sigma(I)$], wR_2 [a]	0.0445, 0.0787	0.0336, 0.0938	0.0524, 0.1091	0.0477, 0.0687
R indices (all data), wR_2 [a]	0.0978, 0.0957	0.0375, 0.0955	0.0716, 0.1121	0.1476, 0.0746
Max./min. Δρ [e·Å^{-3}]	0.519/−0.492	0.391/−0.349	0.476/−0.213	0.326/−0.246
Goodness-of-fit on F^2	1.007	1.024	1.165	0.735

[a] As defined in SHELXL 97-2.

lated. Refinements by full-matrix least-squares calculations[22] on F^2 converged to the indicators given in Table 9. Anisotropic displacement parameters were refined for all atoms heavier than hydrogen. All atomic coordinates and isotropic displacement parameters were refined for the hydrogen atoms of **1b**. Idealised bonds lengths and angles for CH_3, CH_2 and CH groups were used for the other compounds; the riding model was applied for their hydrogen atoms. In addition, the hydrogen atoms of the CH_3 groups were allowed to rotate around the neighbouring C−C bonds. The isotropic displacement parameters of the H atoms were kept equal to 150, 120 and 120% of the equivalent isotropic displacement parameters of the parent primary, secondary and "aromatic" carbon atoms, respectively. Scattering factors, dispersion corrections and absorption coefficients were taken from International Tables for Crystallography (**1992**, Vol. C, Tables 6.1.1.4, 4.2.6.8 and 4.2.4.2). CCDC-197748 to -197751 contain the supplementary crystallographic data for this paper. These data can be obtained free of charge at www.ccdc.cam.ac.uk/conts/retrieving.html [or from the Cambridge Crystallographic Data Centre, 12 Union Road, Cambridge CB2 1EZ, UK; Fax: (internat.) + 44-1223/336-033; E-mail: deposit@ccdc.cam.ac.uk].

Acknowledgments

We thank the Fonds der Chemischen Industrie for the continual support of our work.

[1] W. Kläui, M. Berghahn, G. Rheinwald, H. Lang, *Angew. Chem.* **2000**, *112*, 2590−2592; *Angew. Chem. Int. Ed.* **2000**, *39*, 2464−2466.
[2] The nomenclature used for Tp is based on the one described: S. Trofimenko, *Chem. Rev.* **1993**, 943−980.
[3] S. Trofimenko, J. C. Calabrese, J. S. Thompson, *Inorg. Chem.* **1987**, 1507−1514.
[4] S. Trofimenko, J. C. Calabrese, P. J. Domaille, J. S. Thompson, *Inorg. Chem.* **1989**, 1091−1101.
[5] B. J. Hathaway in *Comprehensive Coordination Chemistry* (Eds.: G. Wilkinson, R. D. Gillard, J. A. McCleverty), Pergamon Press, Oxford, **1987**, vol. 2 ("Ligands").
[6] A. Beck, B. Weibert, N. Burzlaff, *Eur. J. Inorg. Chem.* **2001**, 521−527.
[7] W. Kläui, D. Schramm, W. Peters, G. Rheinwald, H. Lang, *Eur. J. Inorg. Chem.* **2001**, 1415−1424.
[8] R. Han, A. Looney, K. McNeill, G. Parkin, A. L. Rheingold, B. S. Haggerty, *J. Inorg. Biochem.* **1993**, *49*, 105−121.
[9] A. Kremer-Aach, W. Kläui, R. Bell, A. Strerath, H. Wunderlich, D. Mootz, *Inorg. Chem.* **1997**, 1552−1563.
[10] Cambridge Structural Database, Version 5.22, October **2001**.
[11] T. Schönherr, *Top. Curr. Chem.* **1997**, *191*, 87−152.
[12] A. B. P. Lever, *Inorganic Electronic Spectroscopy*, 2nd ed., Elsevier, Amsterdam, **1984**.
[13] T. R. Belderraín, M. Paneque, E. Carmona, E. Gutiérrez-Puebla, M. Angeles Monge, C. Ruiz-Valero, *Inorg. Chem.* **2002**, 425−428 and references therein.
[14] H. Adamsky, M. Atanasov, T. Schönherr, *Comprehensive Coordination Chemistry II* (Eds.: T. J. Meyer, J. A. McClaverty), Elsevier, vol. 1 ("Fundamentals"), in press.
[15] The spin-orbit coupling constant of the free Co^{II} is fairly large (515 cm^{-1}), although it is somewhat reduced in the complex: B. N. Figgis, M. A. Hitchman, *Ligand Field Theory and Its Applications (Special Topics in Inorganic Chemistry)*, John Wiley & Sons, New York, **2000**.
[16] K. Nakamoto, *Infrared and Raman Spectra of Inorganic and Coordination Compounds*, 4th ed., John Wiley & Sons, New York, **1986**.
[17] R. Han, I. B. Gorell, A. Looney, G. Parkin, *J. Chem. Soc., Chem. Commun.* **1991**, 717−719.
[18] [18a] E. Hough, L. K. Hansen, B. Birkness, K. Jynge, S. Hansen, A. Hordvik, C. Little, E. Dodson, Z. Derewenda, *Nature* **1989**, *338*, 357−360. [18b] J. L. Vanhooke, M. M. Benning, F. M. Raushel, H. M. Holden, *Biochemistry* **1996**, *35*, 6020−6025.
[19] H. Günther, *NMR Spectroscopy*, 2nd ed., John Wiley & Sons, New York, **1994**.
[20] D. L. Reger, J. E. Collins, D. L. Jameson, R. K. Castellano, *Inorg. Synth.* **1998**, *32*, 63−65.
[21] G. M. Sheldrick, *SHELXS-97, Program for the Solution of Crystal Structures*, University of Göttingen, Germany, **1990**.
[22] G. M. Sheldrick, *SHELXL-97, Program for the Refinement of Crystal Structures*, University of Göttingen, Germany, **1997**.
[23] M. I. Bruce, A. P. P. Ostazewski, *J. Chem. Soc., Chem. Commun.* **1972**, 1124−1125.
[24] D. L. Reger, J. E. Collins, A. L. Rheingold, L. M. Liable-Sands, *Organometallics* **1996**, *15*, 2029−2032.
[25] C. E. Ruggiero, S. M. Carrier, W. E. Antholine, J. W. Whittaker, C. J. Cramer, W. B. J. Tolman, *J. Am. Chem. Soc.* **1993**, *115*, 11285−11298.
[26] C. Mealli, C. S. Arcus, J. L. Wilkinson, T. J. Marks, J. A. Ibers, *J. Am. Chem. Soc.* **1976**, *98*, 711−718.
[27] N. Kitajima, K. Fujisawa, C. Fujimoto, Y. Moro-oka, S. Hashimoto, T. Kitagawa, K. Toriumi, K. Tatsumi, A. Nakamura, *J. Am. Chem. Soc.* **1992**, *114*, 1277−1291.

Received November 5, 2002

